Remote Sensing of Environment xxx (2015) xxx–xxx

Contents lists available at ScienceDirect

Remote Sensing of Environment

journal homepage: www.elsevier.com/locate/rse

Characterizing residual structure and forest recovery following high-severity fire in the western boreal of Canada using Landsat time-series and airborne lidar data

Douglas K. Bolton [a,*], Nicholas C. Coops [a], Michael A. Wulder [b]

[a] Integrated Remote Sensing Studio, Department of Forest Resources Management, Faculty of Forestry, University of British Columbia, 2424 Main Mall, Vancouver, British Columbia V6T 1Z4, Canada
[b] Canadian Forest Service (Pacific Forestry Centre), Natural Resources Canada, 506 West Burnside Road, Victoria, British Columbia V8Z 1M5, Canada

ARTICLE INFO

Article history:
Received 20 October 2014
Received in revised form 3 March 2015
Accepted 3 March 2015
Available online xxxx

Keywords:
Remote sensing
Disturbance mapping
Forest succession
Structural development
Image classification

ABSTRACT

Post-fire regrowth is an important component of carbon dynamics in Canada's boreal forests, yet observations of structural development following fire are lacking across this remote and expansive region. Here, we used Landsat time-series data (1985–2010) to detect high-severity fires in the Boreal Shield West ecozone of Canada, and assessed post-fire structure for >600 burned patches (>13,000 ha) using airborne light detection and ranging (lidar) data acquired in 2010. We stratified burned areas into patches of dense (>50% canopy cover) and open (20–50% canopy cover) forests based on a classification of pre-fire Landsat imagery, and used these patches to establish a 25-year chronosequence of structural development for each class. While structural attributes were similar between dense and open patches during the first ten years since fire (YSF), canopy cover (cover above 2 m) and stand height (75th height percentile) were significantly higher ($p < 0.001$) for dense patches by the end of the chronosequence (20–25 YSF), suggesting that differences in site productivity were driving patches towards pre-disturbance structure. Our results suggest that growing space remained in stands at the end of the chronosequence, and therefore stem exclusion was not yet reached, as canopy cover was significantly lower ($p < 0.001$) for patches at 20–25 YSF (mean = 41.9% for dense, 18.6% for open) compared to patches with no recorded burns (mean = 63.3% for dense, 38.6% for open). The lasting impact of high-severity fire on structure was further confirmed by estimates of stand height, which were approximately half as tall for patches 20–25 YSF (4.9 m for dense, 4.2 m for open) compared to patches with no recorded burns (9.8 m for dense, 7.7 m for open). Additionally, we assessed the structural complexity of burned stands using measures of canopy roughness (i.e., rumple) and the distribution shape of lidar returns (i.e., skewness and kurtosis), which provided evidence of young, even-aged structure once a new overstory was formed. As forest inventories are not routinely conducted across Canada's northern boreal, the fusion of Landsat time-series and airborne lidar data provides powerful means for assessing changes in forest structure following disturbance over this large forested area.

1. Introduction

An average of two million hectares of forests is burned annually across Canada, with the boreal region accounting for 88% of the documented burned area between 1959 and 1997 (Stocks et al., 2002). These fires lead to significant changes in forest structure, with direct carbon emissions from fire across Canada estimated at 27 Tg carbon year^{-1} (Amiro, Stocks, Alexander, Flannigan, & Wotton, 2001). In the absence of active fire suppression, the northern boreal of Canada is dominated by large, stand-replacing crown fires, typically started by lightning strikes (De Groot et al., 2013; Stocks et al., 2002; Wooster, 2004). As the majority of these northern forests are unmanaged and not subjected to routine forest inventory (Gillis, Omule, & Brierley, 2005), a strong characterization of the impacts of these fires on forest structure is lacking. Additionally, due to the large extent of the northern boreal and the limited access to these forests (Andrew, Wulder, & Coops, 2012), quantifying the structural response to a range of fire events is difficult through field measurement alone.

Landsat data has been used extensively to detect and describe forest disturbances at regional scales for decades (e.g., Cohen et al., 2002; Schroeder, Wulder, Healey, & Moisen, 2011; Vogelmann & Rock, 1988). The change in the normalized burn ratio (NBR) between Landsat images, for example, has been used to detect fires and estimate burn severity (Hall et al., 2008; López García & Caselles, 1991; Soverel, Perrakis, & Coops, 2010). The opening of the Landsat archive in 2008, along with advances in cloud screening (Zhu & Woodcock, 2012) and atmospheric

* Corresponding author. Tel.: +1 604 822 6592; fax: +1 604 822 9106.
E-mail address: doug.k.bolton@alumni.ubc.ca (D.K. Bolton).

http://dx.doi.org/10.1016/j.rse.2015.03.004
0034-4257/

correction (Masek et al., 2006), has led to a drastic increase in the volume of Landsat data used in disturbance detection studies, both spatially and temporally (Wulder, Masek, Cohen, Loveland, & Woodcock, 2012). By developing approaches to analyze dense time-series of Landsat images (e.g., Hermosilla et al., 2015; Huang et al., 2010; Kennedy, Yang, & Cohen, 2010; Zhu, Woodcock, & Olofsson, 2012), it is now possible to reconstruct the history of forest disturbances over the Landsat data record. For example, Goodwin and Collett (2014) processed thousands of images across 20 Landsat scenes to map fire history in Queensland, Australia from 1986 to 2013.

While Landsat is well-suited to detect and describe fires, the lack of three-dimensional information limits our ability to assess the structural response of forests using Landsat data alone. To address this issue, recent attempts have relied on a fusion of Landsat time-series and light detection and ranging (lidar) data, which together provide the means to detect disturbances and quantify their impact on forest structure (Kane et al., 2014; Pflugmacher, Cohen, Kennedy, & Yang, 2014; Wulder et al., 2009). Kane et al. (2013) differentiated the structure of forests following varying levels of burn severity in Yosemite National Park using Landsat data to determine burn severity and airborne lidar to assess structural response. The regeneration of vegetation following disturbance can also be tracked through the fusion of Landsat time-series and lidar data. For example, Lefsky, Turner, Guzy, and Cohen (2005) used Landsat to determine stand age and airborne lidar to assess biomass accumulation and forest productivity in western Oregon. Alternatively, Goetz, Sun, Baccini, and Beck (2010) used spaceborne lidar data acquired by the Geoscience Laser Altimetry System (GLAS) to assess vegetation regrowth following fire over large areas of Alaskan boreal forests.

A range of structural attributes can be estimated from airborne lidar data that are of interest in aboveground biomass and habitat characterization research, such as canopy cover, stand height, and stand structural complexity (Kane, McGaughey et al., 2010; Lefsky, Hudak, Cohen, & Acker, 2005). While estimates of canopy cover and stand height can be estimated directly from a lidar point cloud, structural complexity is often inferred as the variability in return height (Zimble et al., 2003) or the variation in maximum height across the canopy surface (Kane, McGaughey, et al., 2010). In addition, a number of studies have demonstrated the value of lidar data for characterizing forest successional stage (e.g., Falkowski, Evans, Martinuzzi, Gessler, & Hudak, 2009; Kane, Bakker et al., 2010, 2011; Van Ewijk, Treitz, & Scott, 2011). For example, Falkowski et al. (2009) distinguished six stand development stages with over 95% accuracy in northern Idaho, using a range of lidar metrics that described vegetation height and canopy cover. Using lidar metrics to assess successional stage provides powerful means for assessing forest response to disturbance.

In the summer of 2010, transects of small-footprint airborne lidar data were collected across the Canadian boreal, with a total length of approximately 25,000 km. This lidar dataset provides an opportunity to assess the structural response of forests to a range of fire events. Using this dataset, Magnussen and Wulder (2012) developed a relationship between canopy height and time since fire for 163 fires that occurred from 1942 to 2007, which were recorded in the Canadian National Fire Database (CNFDB), a compilation of historical fire data from fire management agencies across Canada. As most fire perimeters in the CNFDB are generalized and can contain a mosaic of burned and unburned forest patches, Magnussen and Wulder (2012) required a statistical approach based on maximum expected growth to separate burned, regenerating vegetation from unburned vegetation within the fire perimeters. Using Landsat time-series data to delineate burned areas in place of the CNFDB would facilitate a more precise assessment of post-burn structure.

In this analysis, we detect high-severity burned patches from 1985 to 2010 using Landsat time-series data across 40 million ha of Canada's Boreal Shield West ecozone, and assess the structural response to these fires using airborne lidar transects. By sampling patches that burned over a 25-year period, we construct a 25-year chronosequence of structural development to address the following questions:

Do lidar metrics capture residual forest structures (e.g., snags, surviving trees) as well as tree regeneration during the first 25 years since fire (YSF)?

High-intensity crown fires, which dominate the Canadian boreal, leave little to no live tree cover in the immediate years following fire (Heinselman, 1981; Viereck, 1983). Before regenerating trees begin to form an overstory, lidar metrics will capture and relate to residual structures such as snags (i.e., standing dead wood) or trees that survive the fire. As tree growth is restricted to short growing seasons (Bonan & Shugart, 1989) and tree establishment can take a number of years following fire in the boreal (Johnstone et al., 2004), we do not expect an overstory to begin forming until at least ten years after fire (e.g., Gralewicz, Nelson, & Wulder, 2012).

How does structure at the end of the chronosequence compare to structure in patches with no record of burning?

In particular, we are interested in observing if stands reach crown closure by the end of the chronosequence (20–25 YSF), and how estimates of stand height, an indicator of aboveground biomass, compare to stands with no record of burning. Harper et al. (2002) found that canopy cover was highest in eastern boreal stands from 50 to 100 YSF, while stand height peaked from 75 to 150 YSF, suggesting that structure at the end of the chronosequence will remain significantly different than in patches with no recorded burns. Additionally, we expect stand structure to be less complex at the end of the chronosequence compared to stands with no record of burning, as canopy breakup and gap filling (Chen & Popadiouk, 2002) lead to more complex canopies in older boreal stands (Brassard, Chen, Wang, & Duinker, 2008).

Does canopy cover prior to fire relate to stand development post-fire?

Site-level conditions and pre-fire stand composition have been shown to strongly influence stand development following fire in boreal forests (e.g., Boucher, Gauthier, & De Grandpré, 2006; Greene et al., 2007; Harper, Bergeron, Drapeau, Gauthier, & De Grandpré, 2005; Johnstone & Chapin, 2006). As structural measurements prior to fire are not available, we will classify burned patches into open (20–50% canopy cover) and dense (>50% canopy cover) forests using pre-fire Landsat imagery. We expect newly established trees to grow faster in patches classified as dense prior to fire, as these sites are likely more productive. However, it is unclear the degree to which structural differences between dense and open patches will be detectable with lidar during the first 25 YSF.

By addressing these questions, we intend to develop improved techniques for assessing structural response to fire and provide an improved characterization of the impacts of fire on forest structure in the Canadian boreal.

2. Methods

2.1. Study area

The Boreal Shield is the largest Canadian ecozone, spanning from Newfoundland in the east to Saskatchewan in the west (Ecological Stratification Working Group, 1995). The ecozone is dominated by coniferous species, such as black spruce (*Picea mariana*), white spruce (*Picea glauca*), and balsam fir (*Abies balsamea*), which are capable of tolerating the long, cold winters of this ecozone. Broadleaf species, such as trembling aspen (*Populus tremuloides*) and white birch (*Betula papyrifera*), are more abundant towards the southern portion of the ecozone (Ecological Stratification Working Group, 1995; Farrar, 1995). As the Boreal Shield spans a wide range of climatic and ecosystem conditions from east to west, the ecozone is often divided into east and west compartments for analysis (Stinson et al., 2011; Stocks et al., 2002). The percent annual area burned between 1959 and 1997 was more than five times higher in the Boreal Shield West (0.76%) compared to the Boreal Shield East (0.15%, Stocks et al., 2002), mainly due to drier conditions in the west and a higher probability of lightning strikes (Brassard &

Please cite this article as: Bolton, D.K., et al., Characterizing residual structure and forest recovery following high-severity fire in the western boreal of Canada using Landsat t..., *Remote Sensing of Environment* (2015), http://dx.doi.org/10.1016/j.rse.2015.03.004

Chen, 2006). Due to this large difference in percent annual area burned, the Boreal Shield West was selected as the focus of this study.

With a relatively short fire cycle in the Boreal Shield West (~130 years based on the above estimate of percent annual area burned), the initial cohort of trees that establishes following fire can dominate a stand until the next stand-replacing disturbance (Johnstone, Hollingsworth, Chapin, & Mack, 2010). Coniferous species establish most sites following fire, with broadleaf establishment restricted to sites with thin organic layers (Greene et al., 2007).

The majority of the Boreal Shield West is 'de facto' protected due to limited human access (Andrew et al., 2012), resulting in an ecozone dominated by natural disturbance processes. In addition to fire, disturbances such as insect defoliation, disease, and windthrow alter forest structure by impacting growth rates and leading to the formation of canopy gaps through tree mortality (Brassard & Chen, 2006; Chen & Popadiouk, 2002). Severe outbreaks of eastern spruce budworm (*Choristoneura fumiferana*) can lead to high rates of tree mortality (Bergeron, Leduc, Morin, & Claude, 1995), such as the large outbreak that impacted over 50 million ha of forests in eastern Canada in the 1970s (Blais, 1983).

2.2. Datasets

2.2.1. Airborne lidar data

The Canadian Forest Service, in collaboration with the Canadian Consortium for Lidar Environmental Applications Research (C-CLEAR) and the Applied Geomatics Research Group, collected 34 transects of small-footprint airborne lidar data over the Canadian boreal in the summer of 2010. The data were collected by an Optech ALTM 3100 discrete return sensor, with a fixed scan angle of 15° and a pulse repetition frequency of 70 kHz between the altitudes of 450 m and 1900 m. The transects totaled ~25,000 km in length, with an average pulse density of 2.8 returns/m^2 and a minimum swath width of 400 m. Preprocessing of the lidar dataset, including the classification of points into ground and non-ground returns, was completed using customized software tools designed to deal with large transect files (Hopkinson et al., 2011). Of the 25,000 km flown, approximately 4500 km falls within the Boreal Shield West.

2.2.2. Landsat data

Thirteen Landsat scenes that intersect the airborne lidar transects within the Boreal Shield West were selected for the analysis (Fig. 1). Landsat scene selection was guided by the Canadian National Fire Database (CNFDB), with selected scenes containing 6–26 fires in the CNFDB which intersected the airborne lidar transects between 1985 and 2010. All available imagery from the Landsat Surface Reflectance Climate Data Record (CDR) collected between June and September of 1984 to 2013 and containing <60% cloud cover were downloaded from earthexplorer.usgs.gov. The CDR consists of Landsat Thematic Mapper (TM) and Enhanced Thematic Mapper (ETM+) data processed to surface reflectance through the Landsat Ecosystem Disturbance Adaptive Processing System (LEDAPS, Masek et al., 2006). Each image in the CDR is delivered with Fmask, a cloud and cloud shadow mask produced at Boston University (Zhu & Woodcock, 2012). The number of downloaded images per scene ranged from 146 to 186 (Table 1). Approximately half the area of the Boreal Shield West was sampled using these 13 Landsat scenes (~40 million ha).

2.2.3. Land cover

To remove wetlands and water from the analysis, information on land cover was obtained from the Earth Observation for Sustainable Development of Forests (EOSD) dataset (http://tree.pfc.forestry.ca/). The circa 2000 land cover dataset, hereafter noted as EOSD LC 2000, is a Landsat-based classification of the forested ecosystems of Canada led by the Canadian Forest Service, with federal, provincial, and university partners. The EOSD LC 2000 products are of a 25 m spatial resolution, following a classification scheme derived from the National Forest Inventory, as well as the information needs of provincial and terrestrial forest management agencies (for additional detail, see Wulder et al., 2008).

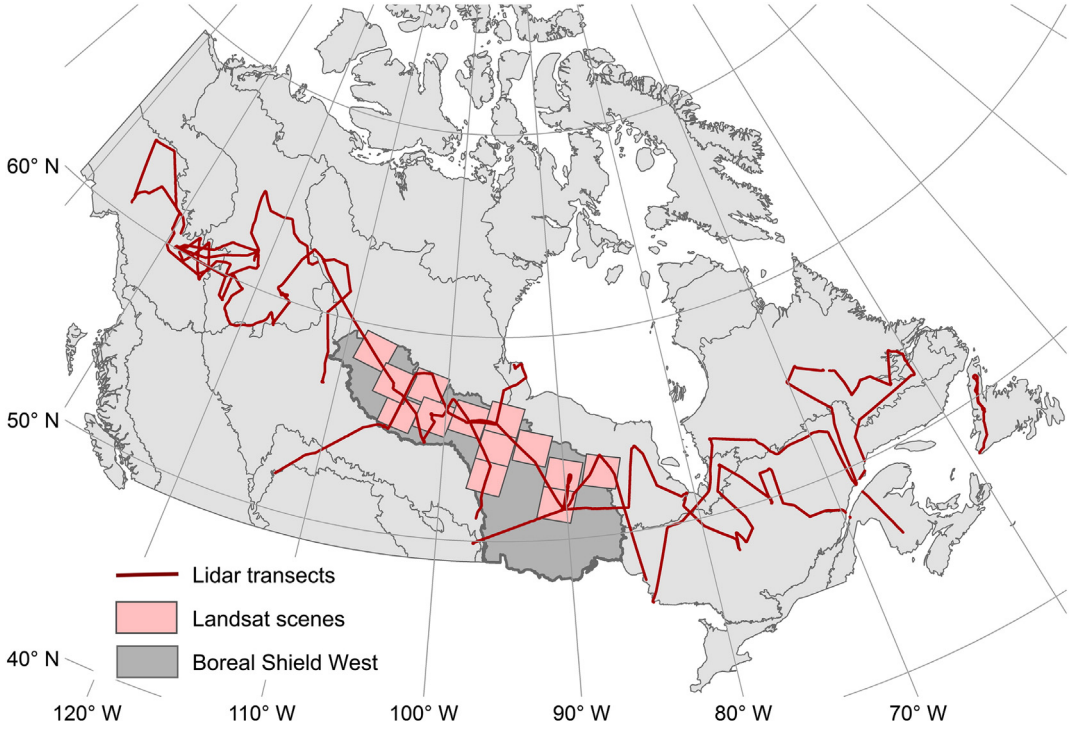

Fig. 1. The airborne lidar transects and selected Landsat scenes overlaid on the terrestrial ecozones of Canada.

Please cite this article as: Bolton, D.K., et al., Characterizing residual structure and forest recovery following high-severity fire in the western boreal of Canada using Landsat t..., *Remote Sensing of Environment* (2015), http://dx.doi.org/10.1016/j.rse.2015.03.004

Table 1
Number of images acquired by path/row between June–Sept 1984–2013.

Path	Row	L5 TM	L7 ETM+	Total
25	23	113	49	162
27	23	109	59	168
27	24	117	55	172
29	22	114	63	177
31	21	104	59	163
31	22	117	54	171
31	23	130	56	186
33	21	111	50	161
35	21	102	56	158
36	20	92	54	146
37	21	117	65	182
38	20	117	49	166
40	19	121	52	173

2.3. Fire detection

The detection of fires was performed on a scene by scene basis, using all Landsat imagery within 45 days of August 1st from 1984 to 2013 (Fig. 2). A 90-day window was selected to maximize the number of Landsat images while avoiding images before vegetation greenup or after vegetation senescence, and reducing images with snow. As fire results in large spectral changes in Landsat time-series analysis, slight variability between images due to phenological differences will have minimal impact on fire detection. Our approach relies on detecting changes in NBR, which is calculated using Landsat band 4 (near-infrared) and band 7 (shortwave-infrared).

$$\mathrm{NBR} = (\mathrm{B4} - \mathrm{B7})/(\mathrm{B4} + \mathrm{B7}) \quad (1)$$

The change in NBR from pre- to post-fire, known as the differenced NBR (dNBR), has been shown to correlate to burn severity (Hall et al., 2008; Soverel et al., 2010).

$$\mathrm{dNBR} = \mathrm{NBR}_{\mathrm{Pre}} - \mathrm{NBR}_{\mathrm{Post}} \quad (2)$$

Healthy vegetation is highly reflective in the near-infrared and absorptive in the mid-infrared, resulting in a drastic change in NBR when vegetation is removed by fire (i.e., decrease in near-infrared reflectance, increase in mid-infrared reflectance). Hall et al. (2008) found a strong relationship ($R^2 = 0.88$) between dNBR and the composite burn index for 161 field plots across four large boreal fires in Saskatchewan, the Northwest Territories, and the Yukon. Based on this relationship, Hall et al. (2008) developed dNBR thresholds for low, moderate, and high severity burns, which were used to detect burned patches in this analysis. Prior to detecting fires with dNBR, a number of pre-processing steps were required.

2.3.1. Generation of Landsat stacks and removal of noise

Landsat data for each scene were stacked using a nearest neighbor resampling. Pixels detected as cloud or cloud shadow by Fmask were masked in each image. Additionally, as pixels in close proximity to clouds can be contaminated or contain undetected cloud edges, any pixel within 500 m of a detected cloud or cloud shadow was removed from the analysis. A water mask was created for each Landsat scene

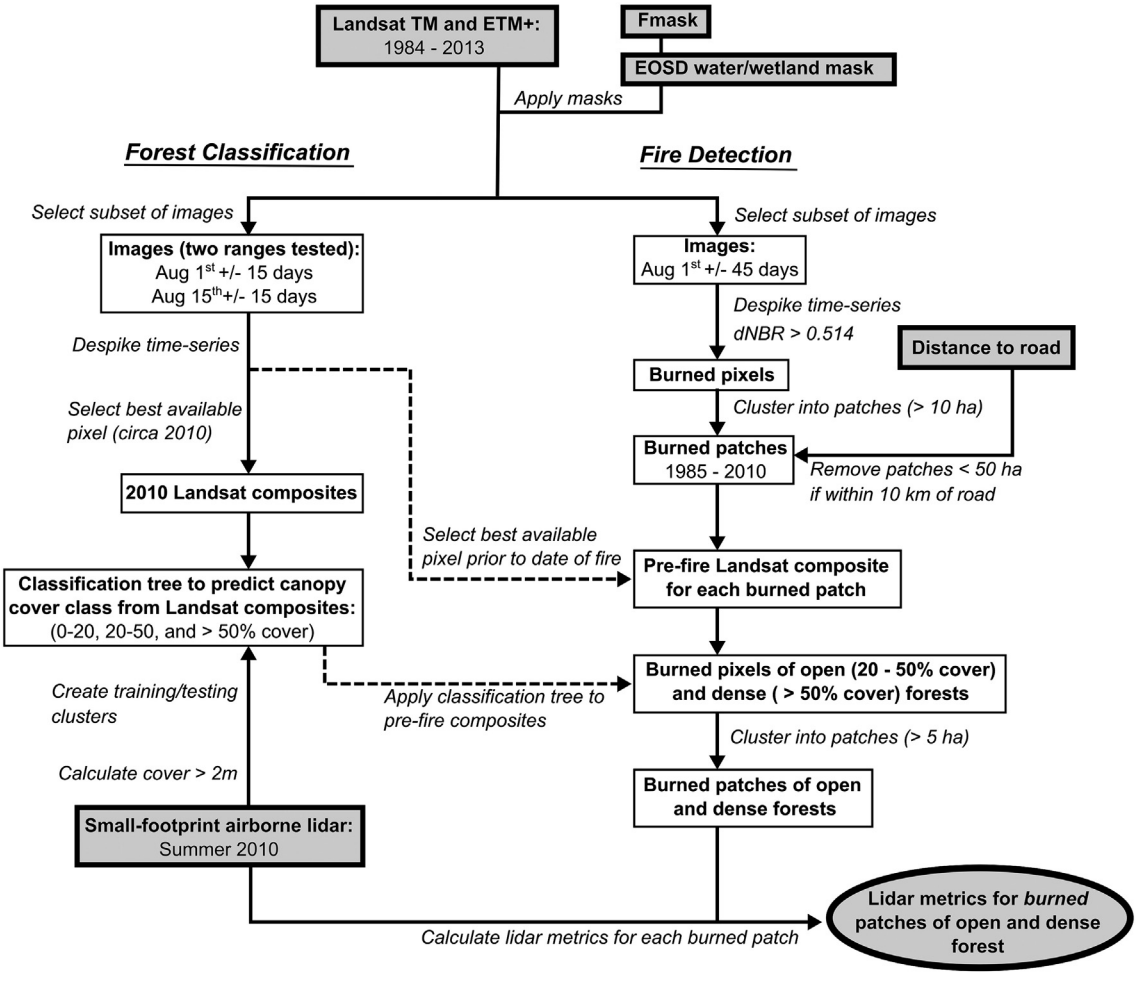

Fig. 2. Flow chart of processing steps to derive lidar metrics for open and dense forest patches that burned between 1985 and 2010. These steps are described in detail in Sections 2.3–2.5.

Please cite this article as: Bolton, D.K., et al., Characterizing residual structure and forest recovery following high-severity fire in the western boreal of Canada using Landsat t..., *Remote Sensing of Environment* (2015), http://dx.doi.org/10.1016/j.rse.2015.03.004

by identifying pixels consistently classified as water by Fmask (>75% of images). Requiring that a pixel was consistently classified as water ensured that a misclassified pixel in one image is not removed unnecessarily. The EOSD LC 2000 dataset was used to mask any remaining water pixels as well as wetland areas from the Landsat stacks.

While most noise associated with clouds and cloud shadows was removed by the above procedures, undetected clouds, cloud shadows, haze, or smoke can lead to the false detection of change in the time-series. While the spectral signal of disturbances likely persists for multiple images, noise will typically result in a "spike" in the time-series. Kennedy et al. (2010) developed a method to detect and remove spikes in Landsat time-series data by testing the similarity of a spectral index before and after the spike in the time-series. Essentially, if the pre- and post-spike values are similar to each other, relative to the magnitude of the spike, then the spike is not considered real change and is removed based on the following equation:

$$\left| \frac{\mathrm{Ind}_{\mathrm{Post}} - \mathrm{Ind}_{\mathrm{Pre}}}{\mathrm{Ind}_{\mathrm{Spike}} - \frac{\mathrm{Ind}_{\mathrm{Post}} + \mathrm{Ind}_{\mathrm{Pre}}}{2}} \right| < 1 - \mathrm{Despike} \quad (3)$$

where Despike is a user-defined threshold which determines how aggressively spikes are removed. Despike can range from 0 to 1, with smaller values resulting in more aggressive despiking. To identify time-series spikes in this analysis, the Kennedy et al. (2010) approach was applied to both NBR and Tasseled Cap Transformation (TCT) brightness component (Crist, 1985). Brightness was included in addition to NBR as it is well suited to capture spikes associated with smoke (which is a common source of noise when detecting fires), as smoke is reflective across all Landsat bands, with greater reflectance found with the shorter, visible, bands. The approach was applied iteratively through the time-series for each pixel, until all spikes were removed using a despike value of 0.75, which was proposed by Kennedy et al. (2010) as an aggressive value for removing time-series spikes.

2.3.2. Detection of burned patches

Following the application of masks and removal of time-series spikes, dNBR was calculated at each image time-step. To limit the false detection of fires (i.e., errors of commission) and to focus on high-severity burns, only pixels meeting the high-severity threshold defined by Hall et al. (2008) were categorized as burned (dNBR >0.514).

Pixels detected as burned within the same year were clustered into burned patches (i.e., pixels neighboring on one of eight sides). If noise (e.g., clouds) occludes a portion of a burned area, a burned patch may be detected as several patches across two or more years. To address this issue, each missing pixel was temporality filled with the next valid pixel in the time-series. If a filled pixel was detected as burned and joined or created a burned patch >10 ha, then the pixel was labeled as burned in the year to which it was moved. To ensure that entire burned patches were not falsely moved to a previous year, we required that >5% of the burn patch be observed in the first year to justify moving pixels.

To remove small-area disturbances and image noise, burned patches <10 ha were removed from the analysis. Additionally, to limit confusion between fire and anthropogenic disturbances (e.g., harvesting), any patch within 10 km of a road was required to be >50 ha for inclusion in the analysis. While potentially removing some fires, this approach ensures that all identified patches are likely fire in origin. The location of roads was determined using the 2010 Road Network File, which is a compilation of all Canadian roads recorded in Statistics Canada's National Geographic Database (Statistics-Canada, 2010). By detecting large, discrete changes in dNBR, confusion between fire and spruce budworm outbreaks should be minimal, as spectral changes associated with repeat defoliation are typically more gradual through time (Meigs, Kennedy, & Cohen, 2011).

In areas of Landsat scene overlap, the same fire events were detected across multiple scenes. Overlapping burned patches that occurred within +/− one year were joined into the same burned patch. The year of the fire was determined as the earliest year of detection between the overlapping scenes.

2.4. Forest classification

To restrict the analysis to forested areas and differentiate the structural response based on pre-fire conditions, information on land cover prior to fire was required. A classification tree was developed which stratified pixels into three canopy cover classes (0–20%, 20–50%, and >50%) based on pre-fire Landsat data. The classification tree was developed using circa 2010 Landsat composites from each Landsat scene, and trained on canopy cover estimates derived from the 2010 airborne lidar transects.

2.4.1. Development of Landsat image composites

A "best available pixel" approach (e.g., Griffiths, van der Linden, Kuemmerle, & Hostert, 2013; White et al., 2014) was employed to generate a circa 2010 image composite for each Landsat scene. Only images within +/− 15 days of a specified target date were used to develop the composites, as phenological stage can significantly influence the spectral characteristics of vegetation (Song & Woodcock, 2003).

Multiple target dates were tested for creating image composites (August 1st and August 15th) to determine which target date produced the highest classification accuracy. To begin, time-series spikes and pixels within 500 m of clouds or shadows were removed for each image following the procedures in Section 2.3.1. Starting in 2010, each pixel in the composite was filled using the closest available image to the target date. If a pixel could not be filled using 2010 data, it was filled with the closest image to the target date in 2009, and so on, back to 2005. A pixel was marked as missing if a change in NBR >0.514 (i.e., the threshold used for fire detection) occurred between the date of the selected image and the target year of the classification (2010).

2.4.2. Selection of training data

Wulder, White et al. (2012) calculated a range of lidar metrics on a 25 m grid along the lidar transects, including an estimate of canopy cover (percentage of first returns above 2 m). These canopy cover estimates were assigned to each overlapping Landsat pixel. Neighboring pixels that belonged to the same canopy cover class (0–20%, 20–50%, and >50%) were then grouped into training clusters. Pixels located at transitions between classes were not included in the training clusters to minimize the impact of any geolocation error and presence of transitional, possibly mixed, classes. Without a water class, water pixels not captured by the applied masks would consistently be classified as >50% canopy cover (i.e., dense, dark vegetation). Therefore, we included clusters of water as training data, which we extracted from the water mask derived in Section 2.3.1. As wetland areas can be structural similar to forested areas but quite different spectrally, pixels classified as wetland in the EOSD LC 2000 were masked from the training data.

To give equal weight to each training cluster, 25 pixels were randomly sampled from each (clusters with less than 25 non-edge pixels were removed). Additionally, to provide a training set that was representative of the sampled landscapes, we randomly sampled training clusters proportionally to the frequency of each class along the lidar transects (Table 2).

2.4.3. Development of classification tree

Landsat bands 3, 4, 5, and 7 and a series of spectral indices were used to develop the classification tree (Table 3). Indices were selected which relate to overall reflectivity (TCT brightness), photosynthetic activity (NDVI), and moisture content (NDMI and NBR). The classification tree was developed in MATLAB using a ten-fold cross validation approach, which consists of randomly dividing the training clusters into ten

Please cite this article as: Bolton, D.K., et al., Characterizing residual structure and forest recovery following high-severity fire in the western boreal of Canada using Landsat t..., *Remote Sensing of Environment* (2015), http://dx.doi.org/10.1016/j.rse.2015.03.004

groups of equal size and iteratively training the classification on nine groups of clusters while testing on the held-out group (see Friedl & Brodley, 1997 for decision tree approaches to classifying remotely sensed imagery). Two classification tree parameters were iteratively varied to test their influence on classification accuracy: the minimum number of observations (pixels) per node and the maximum number of tree splits. Based on the cross-validated results, the best parameters were selected, and the classification was developed using all data.

2.4.4. Application of classification tree

To apply the classification, pre-fire image composites were derived for each burned patch following the procedure above (Section 2.4.1). The target year of each composite was set to the year in which the fire was detected, and filled only with images collected prior to the detection date. The classification tree was then applied to each pre-fire composite. To restrict the analysis to areas that were forested prior to burning, we focused on the 20–50% and >50% canopy cover classes, which we refer to as 'open' and 'dense' forest, respectively.

2.4.5. Identification of unburned forest stands

To compare the structure of burned patches against forest patches with no recorded burns, the classification was applied across the 2010 Landsat composites. Any pixel detected as burned (dNBR >0.514) in the time-series (1985–2010) was masked, as well as any pixel that intersected a fire in the CNFDB prior to 1985. The earliest recorded fire in the CNFDB for the Boreal Shield West occurred in 1948; however, the quality and completeness of fire records in the CNFDB vary through time and between contributing agencies. Pixels with no recorded burns were clustered to create unburned patches of open (20–50% canopy cover) and dense (>50% canopy cover) forests. By applying the classification to the 2010 composites, the selected unburned patches should be spectrally similar to the burned forest patches prior to fire.

2.5. Assessing structural response to fire

Airborne lidar data was extracted and summarized for each burned forest patch using FUSION, a software package produced by the US Forest Service for processing and visualizing lidar data (available at: http://forsys.cfr.washington.edu/fusion/fusionlatest.html). The analysis focused on several lidar metrics which describe canopy cover, stand height, and the distribution shape of lidar returns, which were calculated directly from the point clouds for each patch. Canopy cover was calculated as the percentage of first returns intercepted above 2 m to the total number of first returns, which relates closely to most field definitions of canopy cover (Jennings, Brown, & Sheil, 1999; USDA Forest Service, 2003). Stand height was assessed as the 75th height percentile of first returns. Height percentiles represent a direct measure of vertical structure from lidar that correlate strongly to stand height estimates such as Lorey's height or dominant height (Næsset, 2004; Wulder, Masek, Cohen, Loveland, & Woodcock, 2012, Wulder, White, et al., 2012). The 95th or 99th percentiles were avoided as these are likely more sensitive to residual structure following fire (e.g., snags), while the 75th percentile is more likely to inform on vegetation regrowth. Only returns above 2 m were used in the calculation of the 75th height percentile to remove the impact of returns from low vegetation and the ground.

Table 2
Frequency of each canopy cover class along the lidar transects. Training patches were randomly sampled to match the frequency of each class across the landscape.

Class	Class frequency		Training clusters	
	Pixels	Percent	Patches	Pixels
>50%	451,752	22.7	340	8500
20–50%	504,943	25.4	382	9550
<20%	545,905	27.5	412	10,300
Water	483,587	24.3	364	9100

Table 3
Landsat data inputs to the classification tree.

Inputs	Citation
Landsat bands 3, 4, 5, and 7	–
Tasseled cap brightness	Crist (1985)
Normalized difference vegetation index (NDVI)	Tucker (1979)
Normalized difference moisture index (NDMI)	Gao (1996), Wilson and Sader (2002)
Normalized burn ratio (NBR)	López García and Caselles (1991)

Skewness and kurtosis, metrics describing the shape of a distribution, were also calculated for each lidar point cloud in FUSION. Skewness describes the symmetry of a distribution. Following fire, a positively skewed distribution of lidar returns could signify the presence of several tall, residual trees among a stand dominated by short, regenerating vegetation. Kurtosis describes the peakedness of a distribution. If a stand consists of dense, regenerating vegetation at a uniform height, the distribution of lidar returns would display a strong peak at the height of this dense vegetation (i.e., high kurtosis). Alternatively, if a stand consists of a range of tree heights or the foliage is dispersed over a wide vertical range, the peak of lidar returns would be less well defined (i.e., lower kurtosis). Similar to the calculation of the 75th height percentile, only returns above 2 m were used to calculate skewness and kurtosis.

In addition to point cloud metrics, a canopy height model (CHM) was developed for each burned patch on a 2 m grid in FUSION, representing the tallest vegetation across the landscape. To reduce the influence of edge effects, the CHM was derived using a 10 m buffer around each burned patch and subsequently clipped to the patch boundary.

Rumple, a measure of canopy surface roughness and an indicator of stand structural complexity (Kane, McGaughey, et al., 2010), was also derived in FUSION for each burned patch. Rumple is calculated as the ratio of CHM surface area to the ground area. The surface area of each 2 m pixel in the CHM is calculated by fitting triangles between the center point of the pixel and the center points of all neighboring pixels (Kane, McGaughey, et al., 2010). Only canopy pixels (CHM >2 m) were used to calculate the average rumple across each patch.

Additionally, each CHM cell was stratified by height (0–2, 2–5, >5 m) to represent various layers of the canopy. Clumps within each class were derived by clustering neighboring pixels. Small clumps consisting of less than 5 pixels (20 m^2) were removed from the analysis. The remaining clumps were used to calculate the percentage of area in each height class for each patch.

To provide a structural comparison between burned and unburned patches, lidar metrics were also calculated for all unburned forest patches. Only burned and unburned forest patches for which >5 ha were sampled with the lidar transects were analyzed. Additionally, areas that burned more than once between 1985 and 2010 were masked before the calculation of these lidar metrics, as the structural response of vegetation could be more complicated in these cases.

3. Results

3.1. Detection of fires and classification of forests

Over 30,000 burned patches were detected across the Landsat scenes between 1985 and 2010 (Fig. 3), totaling ~4 million ha or 17.2% of the sampled land area (after water and wetland areas were removed). Approximately 44,000 ha, or 0.2% of the area, was detected as burned more than once between 1985 and 2010.

The highest cross-validated accuracy for detecting canopy cover classes was achieved using a target date of August 15th (87.2%) compared to August 1st (85.8%). Cross-validated error (i.e., the percentage of pixels misclassified in the cross-validation) was lowest when

Please cite this article as: Bolton, D.K., et al., Characterizing residual structure and forest recovery following high-severity fire in the western boreal of Canada using Landsat t..., *Remote Sensing of Environment* (2015), http://dx.doi.org/10.1016/j.rse.2015.03.004

minimum observations per node was set between 100 and 200 (Fig. 4a), and increased sharply when the tree was pruned to fewer than ten branches (Fig. 4b). With an aim of balancing the accuracy and simplicity of the classification tree, minimum observations per node was set to 100, while maximum number of branches was set to 15. This resulted in an overall cross-validated accuracy of 86.7% (Table 4). Of the ~-4 million ha detected as burned, 30.9% was classified as dense forest (>50% canopy cover) prior to burning, 52.9% as open forest (20–50% canopy cover), 15.6% as <20% canopy cover, and <1% as water.

Table 5 displays the number of patches sampled with airborne lidar data for an area >5 ha, with burned patches aggregated into five year since fire (YSF) groups. More open patches (372 burned, 957 unburned) were sampled along the lidar transects than dense patches (234 burned, 629 unburned). The distribution of patches across latitude and longitude varied between the YSF groups (Fig. 5), but had similar trends between dense and open patches, suggesting that the dense and open patches were typically sampled from the same fire events. The number of burned patches sampled with lidar allowed the structural response to fire to be assessed over 13,583 ha of forests.

3.2. Assessment of structure

Mean canopy cover, as estimated with the percentage of first returns above 2 m, was lowest 5–10 YSF for dense forest patches (8.4%) and 5–15 YSF for open forest patches (5.0–5.6%), followed by increasing trends to 20–25 YSF (Fig. 6a). Of the burned groups, mean canopy cover was highest 20–25 YSF for both dense (41.9%) and open (18.6%) patches, but remained significantly lower ($p < 0.001$) than the unburned groups (63.3% for dense and 38.6% for open). Canopy cover was statistically higher ($p < 0.001$) for dense patches compared to open patches in the 10–15 YSF, 20–25 YSF, and unburned groups.

Stand height, as estimated with the 75th height percentile, displayed contrasting trends to canopy cover (Fig. 6b). For dense patches, the 75th height percentile decreased from 0–5 to 10–15 YSF before increasing gradually to the 20–25 YSF group. The 75th height percentile did not show signs of increasing in open patches near the end of the chronosequence. The difference between unburned and 0–5 YSF groups was less pronounced than for canopy cover, with no statistical difference observed between the unburned and 0–5 YSF group for open forests. The 75th height percentile was significantly higher ($p < 0.001$) for dense patches compared to open patches in both the unburned and 20–25 YSF groups. At 20–25 YSF, the mean 75th height percentile was approximately half as tall (4.9 m for dense, 4.2 m for open) as unburned patches (9.8 m for dense, 7.7 m for open). The interquartile range (IQR) of the 75th height percentile was lower for the 15–25 YSF groups (IQR = 0.9–1.1 m) compared with the unburned forest patches (IQR = 2.7 and 2.4 m). While variability was relatively low for the 75th height percentile from 15 to 25 YSF, variability in canopy cover was relatively high in these groups (IQR = 14.4–20.6%). The coefficient of variation (CV), which allows variability to be compared across metrics (i.e., standard deviation divided by the mean), was lower for the 75th height percentile from 15 to 25 YSF (CV = 0.12–0.20) compared to canopy cover (CV = 0.36–1.02).

Skewness was significantly higher ($p < 0.001$) at 10–20 YSF compared to 0–10 YSF and unburned groups for both dense and open patches (Fig. 6c). Skewness increased sharply between 5–10 and 10–15 YSF for dense patches, followed by a decreasing trend to 20–25 YSF. For open patches, the increase in skewness was more gradual from 5–10 to 15–20 YSF. Skewness was significantly higher ($p < 0.001$) for dense patches compared to open at 10–15 YSF, and significantly higher for open patches at 20–25 YSF ($p < 0.01$) and in the unburned groups ($p < 0.001$). For both dense and open patches,

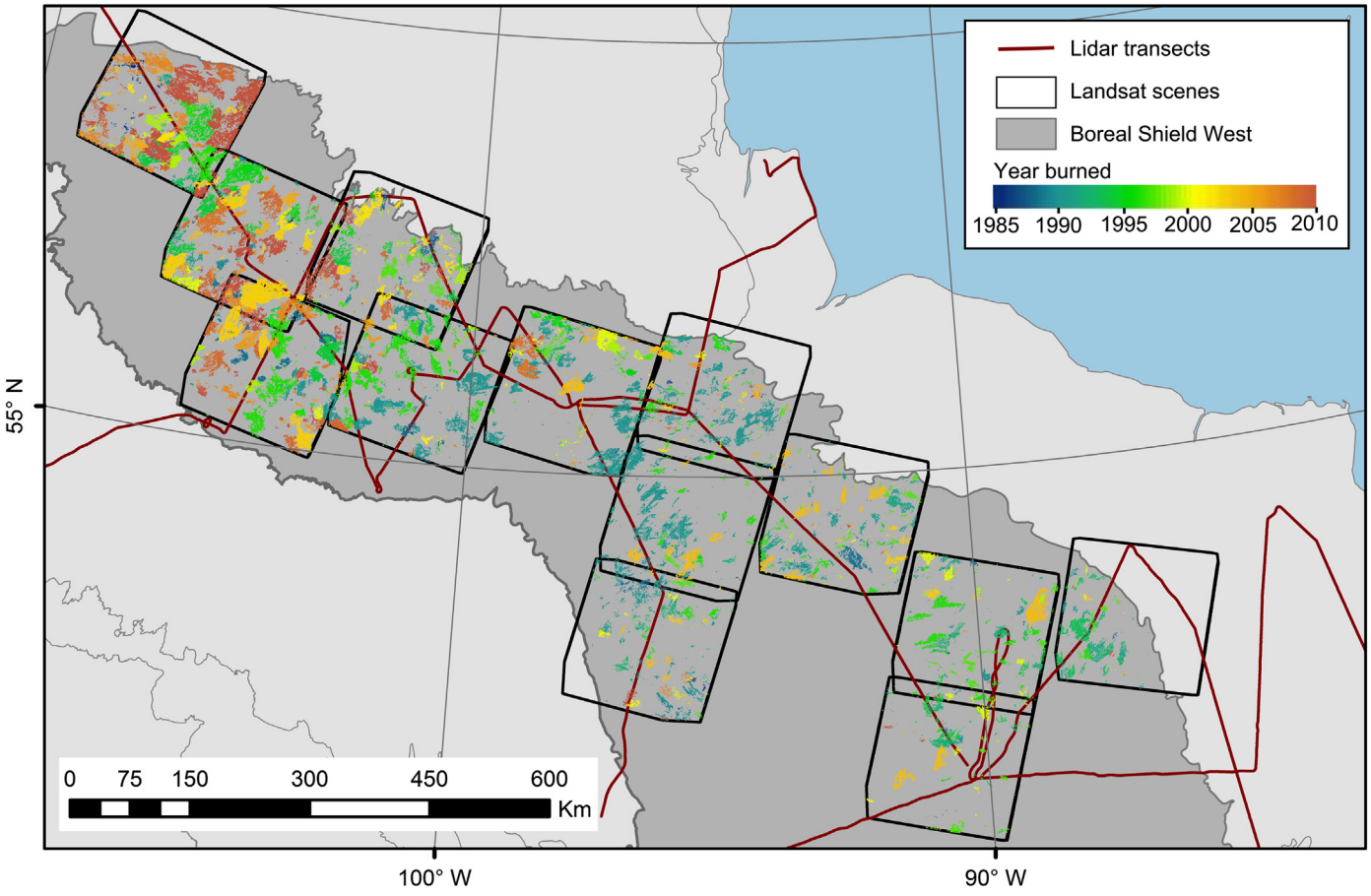

Fig. 3. Burned patches shaded by the year of detection across 13 Landsat scenes.

Please cite this article as: Bolton, D.K., et al., Characterizing residual structure and forest recovery following high-severity fire in the western boreal of Canada using Landsat t..., *Remote Sensing of Environment* (2015), http://dx.doi.org/10.1016/j.rse.2015.03.004

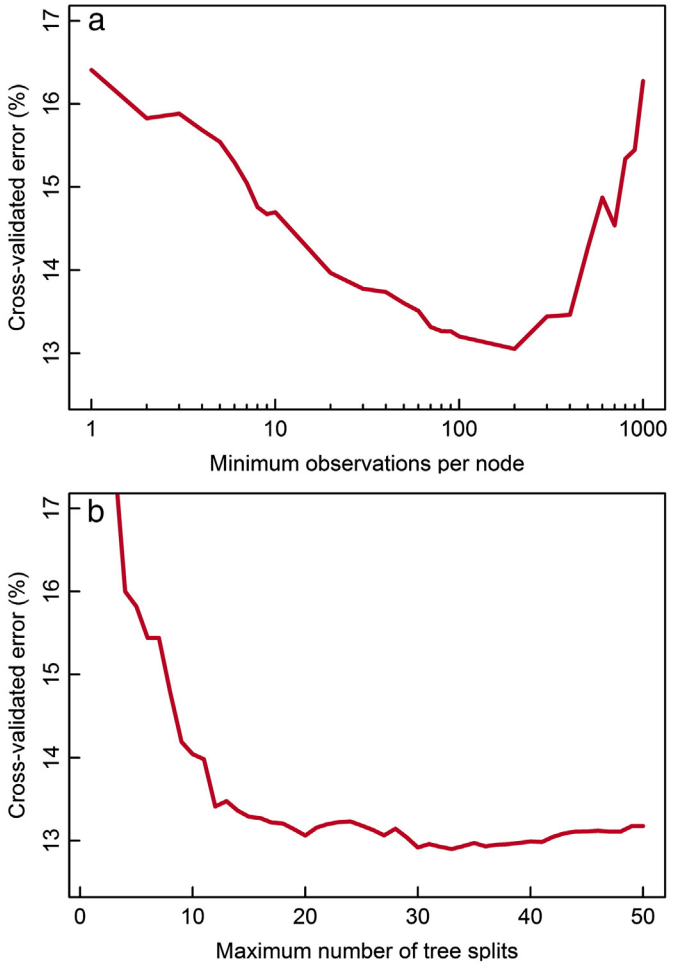

Fig. 4. Cross-validated error using a target date of August 15th for classifying canopy cover as a function of a) minimum observations per node and b) maximum number of tree splits. No tree pruning was used for panel a, while minimum observations per node was set to 100 for panel b.

skewness remained significantly higher ($p < 0.001$) at 20–25 YSF compared to the unburned groups. Skewness was more variable in the 10–25 YSF groups (IQR = 0.88–1.52) compared to the 0–10 YSF and unburned groups (IQR = 0.33–0.48).

The kurtosis, or the strength of the distribution peak of first returns, was significantly higher ($p < 0.001$) 10–25 YSF compared to the 0–10 YSF and unburned groups for both dense and open patches (Fig. 6d). Kurtosis also increased sharply from 5–10 to 10–15 YSF for dense patches, followed by a gradual decrease, while kurtosis increased more gradually for open patches from 5–10 to 15–20 YSF. Kurtosis was

Table 4
Cross-validated accuracy assessment for classifying canopy cover using a single Landsat composite centered on August 15th, 2010. Minimum observations per node set was to 100, and the maximum number of tree splits set to 15. Correctly classified pixels are underlined.

		Reference data (2010 airborne lidar data)				
		>50%[a]	20–50%	<20%	Water	Total
Classified data	>50%	6939	1012	130	20	8101
	20–50%	1410	7220	942	1	9573
	<20%	122	1311	9228	0	10,661
	Water	29	7	0	9079	9115
	Total	8500	9550	10,300	9100	37,450
Producers		81.6	75.6	89.6	99.8	
Users		85.7	75.4	86.6	99.6	
Overall accuracy		86.7				

[a] Percentages represent cover >2 m.

Table 5
The number of dense and open patches sampled with airborne lidar in each YSF group.

Class	Unburned	0–5	5–10	10–15	15–20	20–25 YSF
Dense (>50% cover)	629	27	14	88	53	52
Open (20–50% cover)	957	57	41	126	84	64

significantly higher ($p < 0.01$) for dense patches at 10–15 YSF, while significantly ($p < 0.001$) higher for open patches in the unburned groups. Kurtosis was also more variable in the 10–25 YSF groups (IQR = 5.81–12.17) compared to the 0–10 YSF and unburned groups (IQR = 0.59–1.37).

Fig. 6e displays the rumple of canopy pixels (i.e., pixels >2 m in height) for each YSF group derived from the CHM. The rumple was significantly lower ($p < 0.01$) for the 10–25 YSF groups than 0–10 YSF and unburned groups for both dense and open patches. The mean rumple was highest 0–5 YSF for dense (3.0) and 0–10 YSF for open (2.6–2.8).

Fig. 7 displays the area of the CHM within each height class, expressed as a percentage. The percentage of area below 2 m (i.e., open areas) was highest 5–10 YSF for dense (mean = 83.7%) and 5–15 YSF for open (mean = 88.9–89.9%), followed by a decreasing trend to 20–25 YSF in each case. The area below 2 m remained significantly higher ($p < 0.001$) in dense and open patches at 20–25 YSF compared to the unburned groups. The average area between 2 and 5 m increased from 5–10 to 20–25 YSF for dense (8.8% to 44.1%) and from 10–15 to 20–25 YSF for open (8.7% to 31.2%). For dense patches, the area between 2 and 5 m was more than three times higher 20–25 YSF (mean = 44.1%) compared to unburned (mean = 12.5%). The area above 5 m was relatively high in the first five YSF (mean = 38.3% for dense, 27.1% for open), but decreased sharply by 5–10 YSF (mean = 7.4% for dense, 6.7% for open). The average area above 5 m increased for dense patches from 15–20 to 20–25 YSF (7.7% to 23.4%), but remained significantly lower ($p < 0.001$) than unburned patches (75.9%). No significant increase was observed in the area above 5 m for open patches at the end of the chronosequence.

4. Discussion

The integration of historical disturbance detection from Landsat and structural measurements from lidar provides powerful means for characterizing the response of forests to disturbance over large areas (Kane et al., 2013, 2014). As lidar structural measurements were limited to a single snapshot in time (summer 2010), pre- and post-burn structures could not be directly compared. Therefore, we demonstrated an approach that relies on pre-fire spectral information from Landsat to differentiate varying levels of canopy cover prior to disturbance. By comparing structural attributes from burned stands against those from spectrally similar unburned stands, the impacts of fire on structure could be assessed.

Statistical differences in structural attributes between unburned and 20–25 YSF patches confirm the significant and lasting impact of high-severity fire on structure in the Boreal Shield West. In addition, our results demonstrate the large proportion of the landscape impacted by these burns (17.2% of the sampled area over 25 years, or 0.69%/year). Stocks et al. (2002) found a similar burn rate for the Boreal Shield West (0.76%/year) between 1959 and 1997, however several key differences exist between the estimates: 1) our estimates are for 13 Landsat scenes and not the entire ecozone, 2) we only consider burn patches that met the high-severity threshold defined by Hall et al. (2008), and 3) Stocks et al. (2002) only consider burns >200 ha.

4.1. Structural development following fire

Forest structure immediately following stand-replacing fire is characterized by standing dead wood (i.e., snags) and little to no live tree

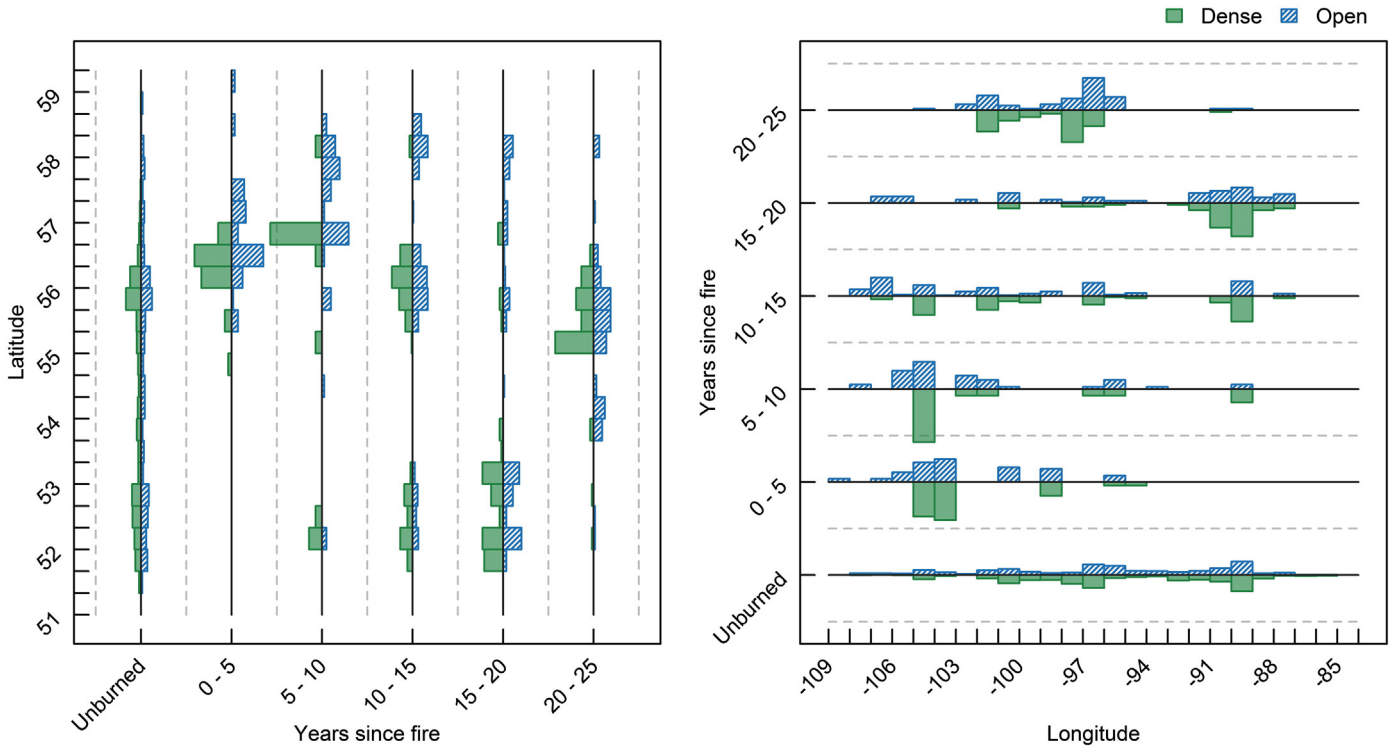

Fig. 5. Distribution of sampled dense and open patches across latitude and longitude. Dashed gray line represents 50% of the data.

cover. Over time, the open space created by the disturbance is filled with new vegetation and standing dead wood begins to fall (Chen & Popadiouk, 2002; Oliver & Larson, 1996). This transition from a canopy of residual structures (i.e., snags or surviving trees) to one dominated by young, even-aged trees was captured clearly by lidar metrics during the 25-year chronosequence.

In the first decade following fire, canopies remained relatively open (i.e., low canopy cover), as most regenerating trees remained below 2 m in height. Slow boreal growth rates and delayed tree establishment would prevent most trees from growing more than 2 m in height during this short time span (Bonan & Shugart, 1989; Johnstone et al., 2004; Sirois & Payette, 1989). At boreal sites in Alaska and the Yukon, Johnstone et al. (2004) found that most trees took 3–7 years to establish following fire. Therefore, instead of detecting new tree growth, lidar metrics were sensitive to residual canopy structures in the first ten YSF. Specifically, the 75th height percentile provided evidence of tall residual trees, as regenerating trees could not achieve the observed heights in less than ten years. The loss of residual structure through time was captured by the CHM metrics, as the percentage of area above 5 m decreased sharply from 0–5 to 5–10 YSF (Angers, Gauthier, Drapeau, Jayen, & Bergeron, 2011; Bond-Lamberty & Gower, 2008). This loss of residual structure as snags begin to fall, in addition to new tree growth above 2 m in height, explains the decreasing trend in the 75th height percentile from 0 - 5 YSF to 10–15 YSF.

From 10 to 25 YSF, estimates of canopy cover and stand height captured the emergence and growth of new trees into the canopy. While dense and open patches were structurally similar in the first ten YSF, estimates of canopy cover and stand height were statistically higher in dense patches by 20–25 YSF, suggesting faster growth and recovery of trees compared to open patches. Growth rates were slow enough in open patches that increases in the 75th height percentile were not observable during the 25-year chronosequence (i.e., the 75th height percentile remained sensitive to residual structure). While temperature is the main limiting factor to growth in most boreal forests, the location of a stand in the landscape can influence the availability of water, nutrients, and sunlight (i.e., slope and aspect), leading to local variations in site productivity (Bonan & Shugart, 1989; Boucher et al., 2006). The classification of patches into dense or open forest appears to have captured some of the underlying differences in site productivity and stand development across the landscape. Specifically, the factors that limited growth prior to disturbance, which determined if a patch was classified as dense or open forest, were also limiting the growth of new trees following fire. As dense and open patches were typically sampled from the same fire events (see Fig. 5), these results suggest that a range of structural responses can be observed within individual fires depending on variations in site-level conditions. Differences in growth rates between dense and open patches were further confirmed by CHM metrics, as considerably more canopy area was above 5 m in height in dense patches at 20–25 YSF compared to open patches. These findings suggest that forest productivity prior to stand-replacing fire, as inferred using pre-disturbance Landsat imagery, is an important indicator of structural response post-fire.

Variability in species composition across the landscape could also contribute to the structural differences observed between dense and open patches. For example, canopy closure would be reached faster in stands dominated by trembling aspen compared to black spruce, due to differences in species growth rates (Chen & Popadiouk, 2002; Johnstone et al., 2004). As tree establishment post-fire is strongly linked to pre-fire species composition (Johnstone & Chapin, 2006; Johnstone et al., 2010), structural differences between stands due to species composition could re-develop during the early stages of succession.

When the open space created by a disturbance is filled, stand initiation is complete, and established trees begin to compete for available sunlight and nutrients (Chen & Popadiouk, 2002; Oliver & Larson, 1996). Our finding that canopy cover remained significantly lower 20–25 YSF compared to stands with no record of burning suggests that available growing space remained at the end of the chronosequence and stem exclusion had not yet been reached. Higher percentages of open areas (CHM <2 m) at 20–25 YSF compared to patches with no recorded burns provide further evidence that available growing space remained. Harper et al. (2005) found that stand initiation lasted 34–39 years in black spruce boreal forests in Ontario, while Lieffers,

Please cite this article as: Bolton, D.K., et al., Characterizing residual structure and forest recovery following high-severity fire in the western boreal of Canada using Landsat t..., *Remote Sensing of Environment* (2015), http://dx.doi.org/10.1016/j.rse.2015.03.004

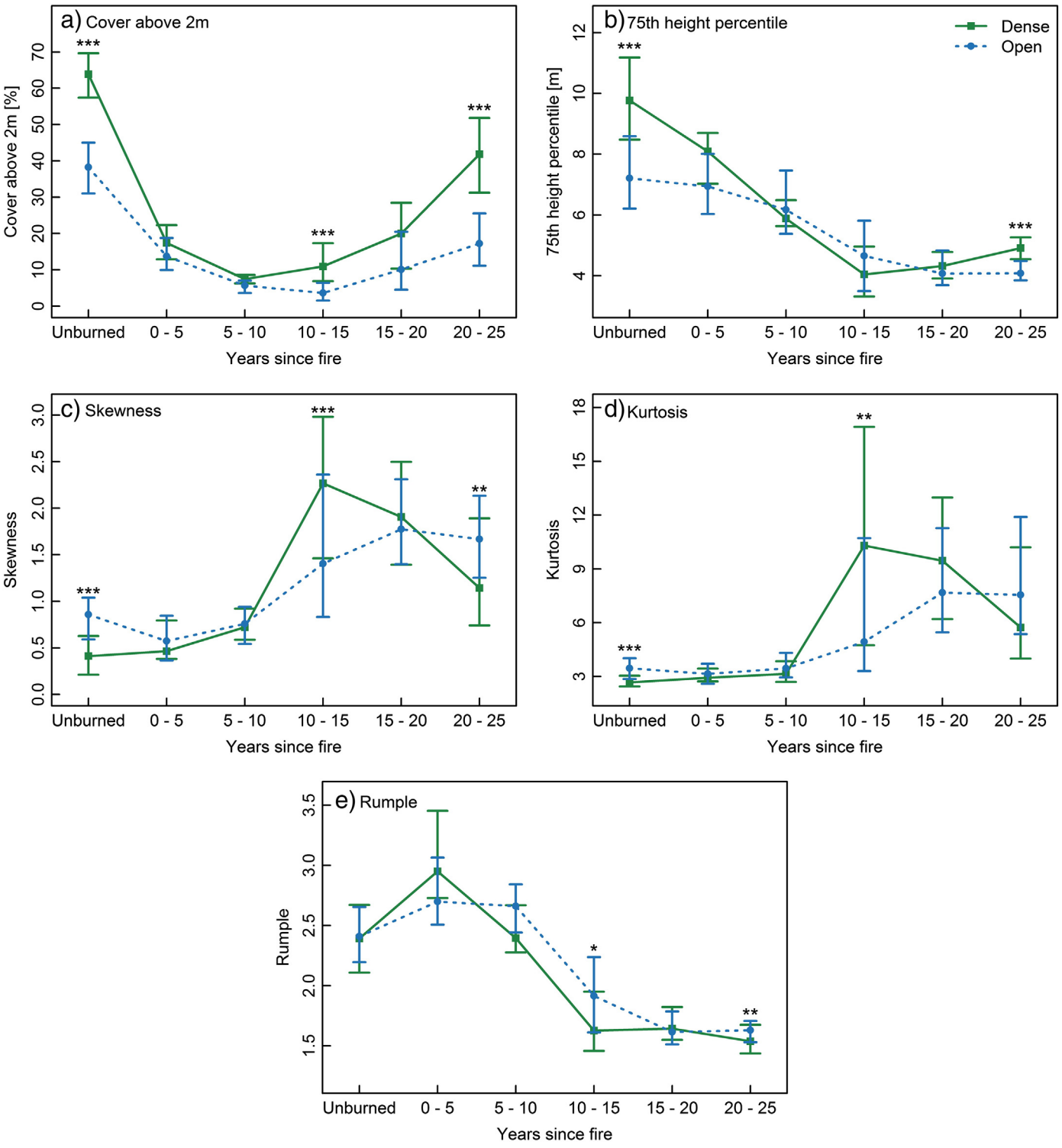

Fig. 6. Median lidar metrics for dense and open patches in each YSF group, with error bars displaying the interquartile range. Rumple was derived from canopy pixels (CHM height >2 m) only. Asterisks represent the statistical differences between dense and open patches in each group (*p < 0.05, **p < 0.01, ***p < 0.001).

Messier, Burton, Ruel, and Grover (2003) suggest 5–15 years for aspen or pine dominated boreal stands and up to 40 years for boreal stands dominated by spruce. Using lidar metrics to assess successional stage in Pacific Northwest forests, Kane et al. (2011) found that canopies in the stem exclusion stage were homogenous and contained relatively few gaps. Most patches did not reach this structural definition of stem exclusion by the end of the chronosequence, as CHMs remained relatively open. However, it should be noted that site limitations on establishment and growth may prevent stands from reaching canopy closure for many decades, if at all, in low productivity boreal stands (Harper et al., 2005). In these cases, competition for other resources besides sunlight (e.g., nutrients and water) may lead to stem exclusion before canopy closure is reached (Carleton & Wannamakerf, 1987). The availability of growing space is therefore only one indicator of the transition from the stand initiation to stem exclusion stage of succession.

Stands typically maintain an even-aged structure for many years following fire, until shade-tolerant trees establish in the understory and trees in the initial cohort begin to die (Chen & Popadiouk, 2002;

Please cite this article as: Bolton, D.K., et al., Characterizing residual structure and forest recovery following high-severity fire in the western boreal of Canada using Landsat t..., *Remote Sensing of Environment* (2015), http://dx.doi.org/10.1016/j.rse.2015.03.004

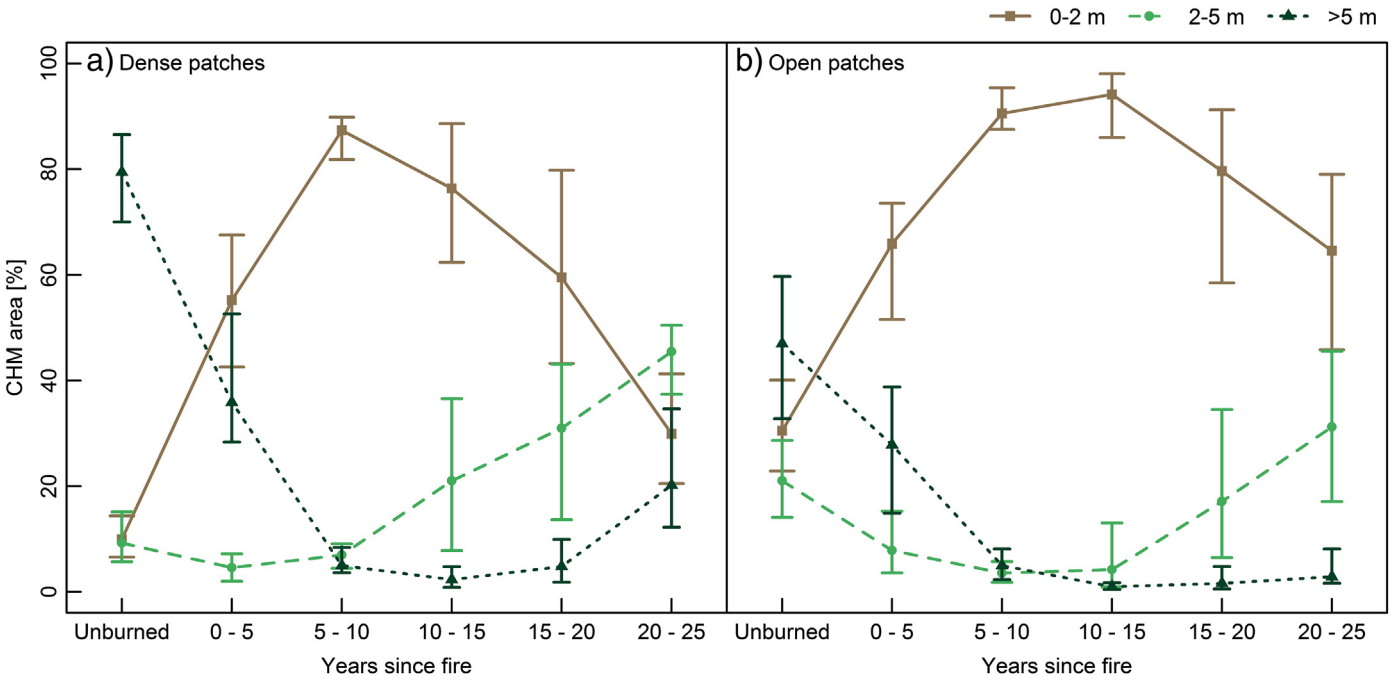

Fig. 7. Median percentage of CHM area in each height class, with error bars displaying the interquartile range, for a) dense and b) open patches. Only clumps >=5 pixels (20 m2) were included in the area calculation.

Oliver & Larson, 1996). The even-aged nature of regenerating trees was first observed at 10–15 YSF, when lidar metrics began to describe the young, emerging canopy. At this time, kurtosis increased sharply in dense patches, suggesting a strong peak in lidar returns from vegetation at a uniform height. Skewness also increased sharply for dense patches at 10–15 YSF, as the combination of short, dense vegetation and tall, sparse vegetation (i.e., residual vegetation) led to positively skewed distributions of lidar returns. Slower growth rates and less dense vegetation explain why skewness and kurtosis increased later, and not as sharply, in open patches. As time since fire increases and trees grow taller, foliage becomes more dispersed vertically, explaining why kurtosis decreased in dense patches at 20–25 YSF. Skewness also decreased in dense patches by the end of the chronosequence, as a smaller proportion of lidar returns will be from residual structures as the density of new trees increases, and snags continue to fall. The length of time that boreal snags remain standing varies widely in the literature (e.g., Angers et al., 2011; Bond-Lamberty & Gower, 2008; Boulanger & Sirois, 2006). For example, Angers et al. (2011) reported a half-life (i.e., length of time for half of snags to fall after mortality) of 4.4 years while Boulanger and Sirois (2006) reported 16.2 years for black spruce in Quebec following fire. This variability in snag persistence, in addition to variability in tree survival, may contribute to the high variability (i.e., high interquartile range) observed within groups for skewness and kurtosis between 10 and 25 YSF. Low skewness for unburned stands suggests that vegetation elements are more normally or evenly distributed in the canopy than in recently burned patches, while low kurtosis suggests that vegetation elements are spread over a wide vertical range, either due to a range of tree heights or a broad canopy layer. Van Ewijk et al. (2011) noted a similar difference in the vertical distribution of lidar returns between early and late successional stands in central Ontario.

Tree size diversity is low in early successional stands, as trees are even-aged and maximum tree size is limited by a short growth period (Boucher et al., 2006; Bradford & Kastendick, 2010). Through time, tree size diversity increases, as differences in growth rates become more pronounced (Boucher et al., 2006), and tree mortality and gap forming disturbances lead to un-even aged structures (Brassard et al., 2008; Chen & Popadiouk, 2002). Rumple, a metric that assesses the roughness of the canopy surface, provided evidence of this contrast in stand complexity between early successional stands and stands with no record of burning. Specifically, low rumple values from 10 to 25 YSF indicate homogenous structure across the young, regenerating stands, while higher rumple values indicate more complex canopy surfaces in patches with no recorded burns. From 0 to 10 YSF, rumple captured the large contrast in height between tall, residual vegetation and surrounding open areas. In the presence of canopy gaps, the height of a stand can influence the rumple (i.e., larger distance from canopy to ground), which could contribute to the differences in rumple observed between early successional stands and stands with no record of burning. In the Pacific Northwest, Kane, Bakker et al. (2010) also found early successional stands to be less complex than late successional stands using the rumple metric.

If the majority of trees in early successional stands occupy a narrow range in size, we would expect low variability in stand height between stands as well. This was the case in this analysis, as within-group variability was low for the 75th height percentile in the 15–20 YSF and 20–25 YSF groups (i.e., low interquartile range). On the other hand, variability in canopy cover was relatively high in the 15–20 YSF and 20–25 YSF groups, as differences in tree establishment (i.e., number and density of trees) and the timing of tree emergence into the canopy can quickly lead to structural differences between canopies (Chen & Popadiouk, 2002; Greene, Noël, Bergeron, Rousseau, & Gauthier, 2004; Johnstone et al., 2004). A range of factors can influence tree establishment following fire, such as the availability of seed sources, the suitability of a site for growth, and the severity of the fire (Greene et al., 2004; Johnstone et al., 2004). These results suggest that cover metrics capture more variability between stands than height metrics in early stand development in boreal forests, due to the low diversity in tree size but potentially large diversity in tree number and density.

Variability in stand height was inherently higher in the unburned groups, as these groups contain a wide range of stand ages. While age was unknown for these patches, we expect that most stands were at least older than 25 years and younger than 130 years (i.e., the approximate fire cycle length for the Boreal Shield West, derived from the results of Stocks et al., 2002). Stochastic processes, such as disturbance

and tree mortality, also contribute to higher structural variability between these older stands (Chen & Popadiouk, 2002; Oliver & Larson, 1996).

4.2. Considerations

Post-fire structural development depends largely on fire severity (Angers et al., 2011; Greene et al., 2004). As the Canadian boreal is dominated by large, stand-replacing crown fires (Heinselman, 1981; Viereck, 1983), we aimed to characterize the response of structure to severe fires only, which we accomplished by applying a dNBR threshold for high-severity fire (Hall et al., 2008). While Hall et al. (2008) found a strong relationship between dNBR and fire severity, a number of factors can confound this relationship, such as the length of time between pre- and post-fire imagery, pre-fire vegetation characteristics, and variation in vegetation and soil moisture (Epting, Verbyla, & Sorbel, 2005; Wulder et al., 2009). Additionally, the assessment of fire severity itself is a highly subjective process, as fire severity is an interpretation of a fire's impact on the environment, not a direct measure (Hall et al., 2008; Lentile et al., 2006). Therefore, while a single dNBR threshold was applied to detect high-severity fires, a range of fire severities may be included in this analysis, contributing to the variability in structural responses observed. Our results suggest that most sampled patches did endure high-severity, stand replacing fires, and the high percentage of the study area impacted by these fires (17.2% in 25 years) demonstrates their significance across the landscape. However, this focus on high severity fire and the potential for confusion between severity classes should be considered when interpreting the results of this study.

5. Conclusions

In this study, we assessed structural development following fire for over 13,000 ha of forests in the Boreal Shield West using a combination of Landsat time-series and airborne lidar data. The lasting impact of fire on forest structure was confirmed by the significant differences ($p < 0.001$) in structure between stands at 20–25 YSF and stands with no record of burning. Our results demonstrate that structural development following fire is highly variable across boreal landscapes, as site conditions, species composition, and fire severity can vary both within and between fires (Bonan & Shugart, 1989; Greene et al., 2004; Johnstone et al., 2004). A spatially explicit understanding of this variability in structural development, both within and between disturbance events, is required to improve characterizations of carbon loss and uptake across forested landscapes. This is of particular importance in high latitude forests, where local variation in received solar radiation and permafrost contributes to a high diversity of site conditions (Bonan & Shugart, 1989). Our results suggest that pre-disturbance conditions are a strong indicator of stand development following fire, as patches classified as dense forest prior to burning displayed faster growth and recovery than patches classified as open forest. Knowledge of pre-disturbance conditions and expected growth can therefore lead to more spatially explicit predictions of stand development and carbon uptake following disturbance.

During the 25-year chronosequence, we observed the transition from open canopies of residual structures to canopies dominated by young, even-aged trees. As the length of the Landsat record continues to grow, we will be able to monitor stands at later stages of succession using this approach, leading to even stronger, more graduated and detailed, characterizations of structural development following disturbance.

Acknowledgments

Three anonymous reviewers are thanked for their time and exceedingly helpful and collegial recommendations that led to the development of an improved manuscript. Dr. Brad Hawkes, of the Canadian Forest Service, is also thanked for a number of thoughtful and insightful suggestions. This research was undertaken as part of the "National Terrestrial Ecosystem Monitoring System (NTEMS): Timely and detailed national cross-sector monitoring for Canada" project jointly funded by the Canadian Space Agency (CSA) Government Related Initiatives Program (GRIP) and the Canadian Forest Service (CFS) of Natural Resources Canada. Components of this research were also funded by a NSERC discovery grant to Nicholas Coops and a graduate fellowship to Douglas Bolton. Chris Hopkinson (previously of Nova Scotia Community College and now with the University of Lethbridge) is thanked for his transect project partnership and his leadership of the national Canadian Consortium for Lidar Environmental Applications Research (C-CLEAR) which was critical in obtaining the research data used in this study. Christopher Bater (previously of UBC and now with the Government of Alberta) is thanked for his analysis efforts and insights into the processing of the lidar transects. Trevor Milne of Gaiamatics is thanked for assisting with the development of customized code for processing the long lidar transect files.

References

Amiro, B.D., Stocks, B.J., Alexander, M.E., Flannigan, M.D., & Wotton, B.M. (2001). Fire, climate change, carbon and fuel management in the Canadian boreal forest. *International Journal of Wildland Fire*, *10*, 405–413.

Andrew, M.E., Wulder, M.A., & Coops, N.C. (2012). Identification of de facto protected areas in boreal Canada. *Biological Conservation*, *146*, 97–107.

Angers, V.A., Gauthier, S., Drapeau, P., Jayen, K., & Bergeron, Y. (2011). Tree mortality and snag dynamics in North American boreal tree species after a wildfire: A long-term study. *International Journal of Wildland Fire*, *20*, 751–763.

Bergeron, Y., Leduc, A., Morin, H., & Claude, J. (1995). Balsam fir mortality following the last spruce budworm outbreak in northwestern Quebec. *Canadian Journal of Forest Research*, *25*, 1375–1384.

Blais, J.R. (1983). Trends in the frequency, extent, and severity of spruce budworm outbreaks in eastern Canada. *Canadian Journal of Forest Research*, *13*, 539–547.

Bonan, G.B., & Shugart, H.H. (1989). Environmental factors and ecological processes in boreal forests. *Annual Review of Ecology and Systematics*, *20*, 1–28.

Bond-Lamberty, B., & Gower, S.T. (2008). Decomposition and fragmentation of coarse woody debris: Re-visiting a boreal black spruce chronosequence. *Ecosystems*, *11*, 831–840.

Boucher, D., Gauthier, S., & De Grandpré, L. (2006). Structural changes in coniferous stands along a chronosequence and a productivity gradient in the northeastern boreal forest of Québec. *Ecoscience*, *13*, 172–180.

Boulanger, Y., & Sirois, L. (2006). Postfire dynamics of black spruce coarse woody debris in northern boreal forest of Quebec. *Canadian Journal of Forest Research*, *36*, 1770–1780.

Bradford, J.B., & Kastendick, D.N. (2010). Age-related patterns of forest complexity and carbon storage in pine and aspen–birch ecosystems of northern Minnesota, USA. *Canadian Journal of Forest Research*, *40*, 401–409.

Brassard, B.W., & Chen, H.Y.H. (2006). Stand structural dynamics of North American boreal forests. *Critical Reviews in Plant Sciences*, *25*, 115–137.

Brassard, B.W., Chen, H.Y.H., Wang, J.R., & Duinker, P.N. (2008). Effects of time since stand-replacing fire and overstory composition on live-tree structural diversity in the boreal forest of central Canada. *Canadian Journal of Forest Research*, *38*, 52–62.

Carleton, T.J., & Wannamakerf, B.A. (1987). *Mortality and self-thinning in postfire black spruce*, *59*. (pp. 621–628), 621–628.

Chen, H.Y.H., & Popadiouk, R.V. (2002). Dynamics of North American boreal mixedwoods. *Environmental Reviews*, *10*, 137–166.

Cohen, W.B., Spies, T.A., Alig, R.J., Oetter, D.R., Maiersperger, T.K., & Fiorella, M. (2002). Characterizing 23 years (1972–95) of stand replacement disturbance in western Oregon forests with Landsat imagery. *Ecosystems*, *5*, 122–137.

Crist, E.P. (1985). A TM tasseled cap equivalent transformation for reflectance factor data. *Remote Sensing of Environment*, *17*, 301–306.

De Groot, W.J., Cantin, A.S., Flannigan, M.D., Soja, A.J., Gowman, L.M., & Newbery, A. (2013). A comparison of Canadian and Russian boreal forest fire regimes. *Forest Ecology and Management*, *294*, 23–34.

Ecological Stratification Working Group (1995). *A national ecological framework for Canada*. Centre for Land and Biological Resources Research, Research Branch, Agriculture and Agri-food Canada.

Epting, J., Verbyla, D., & Sorbel, B. (2005). Evaluation of remotely sensed indices for assessing burn severity in interior Alaska using Landsat TM and ETM+. *Remote Sensing of Environment*, *96*, 328–339.

Falkowski, M.J., Evans, J.S., Martinuzzi, S., Gessler, P.E., & Hudak, A.T. (2009). Characterizing forest succession with lidar data: An evaluation for the Inland Northwest, USA. *Remote Sensing of Environment*, *113*, 946–956.

Farrar, J.L. (1995). *Trees in Canada*. Markham, Ontario: Fitzhenry and Whiteside Ltd (Natural Resources Canada, Canada Forest Service, Ottawa, Ontario).

Friedl, M.A., & Brodley, C.E. (1997). Decision tree classification of land cover from remotely sensed data. *Remote Sensing of Environment*, *61*, 399–409.

Gao, B. -C. (1996). NDWI — A normalized difference water index for remote sensing of vegetation liquid water from space. *Remote Sensing of Environment*, *58*, 257–266.

Please cite this article as: Bolton, D.K., et al., Characterizing residual structure and forest recovery following high-severity fire in the western boreal of Canada using Landsat t..., *Remote Sensing of Environment* (2015), http://dx.doi.org/10.1016/j.rse.2015.03.004

Gillis, M.D., Omule, A.Y., & Brierley, T. (2005). Monitoring Canada's forests: The National Forest Inventory. *The Forestry Chronicle*, *81*, 214–221.

Goetz, S.J., Sun, M., Baccini, A., & Beck, P.S.A. (2010). Synergistic use of spaceborne lidar and optical imagery for assessing forest disturbance: An Alaska case study. *Journal of Geophysical Research*, *115*, 1–14.

Goodwin, N.R., & Collett, L.J. (2014). Development of an automated method for mapping fire history captured in Landsat TM and ETM+ time series across Queensland, Australia. *Remote Sensing of Environment*, *148*, 206–221.

Gralewicz, N.J., Nelson, T.A., & Wulder, M.A. (2012). Factors influencing national scale wildfire susceptibility in Canada. *Forest Ecology and Management*, *265*, 20–29.

Greene, D.F., Macdonald, S.E., Haeussler, S., Domenicano, S., Noël, J., Jayen, K., et al. (2007). The reduction of organic-layer depth by wildfire in the North American boreal forest and its effect on tree recruitment by seed. *Canadian Journal of Forest Research*, *37*, 1012–1023.

Greene, D.F., Noël, J., Bergeron, Y., Rousseau, M., & Gauthier, S. (2004). Recruitment of *Picea mariana*, *Pinus banksiana*, and *Populus tremuloides* across a burn severity gradient following wildfire in the southern boreal forest of Quebec. *Canadian Journal of Forest Research*, *34*, 1845–1857.

Griffiths, P., van der Linden, S., Kuemmerle, T., & Hostert, P. (2013). A pixel-based Landsat compositing algorithm for large area land cover mapping. *IEEE Journal of Selected Topics in Applied Earth Observations and Remote Sensing*, *6*, 2088–2101.

Hall, R.J., Freeburn, J.T., de Groot, W.J., Pritchard, J.M., Lynham, T.J., & Landry, R. (2008). Remote sensing of burn severity: Experience from western Canada boreal fires. *International Journal of Wildland Fire*, *17*, 476–489.

Harper, K. A., Bergeron, Y., Gauthier, S., & Drapeau, P. (2002). Post-fire development of canopy structure and composition in black spruce forests of Abitibi. *Québec: a landscape scale study*, *36*. (pp. 249–263). Silva Fennica.

Harper, K.A., Bergeron, Y., Drapeau, P., Gauthier, S., & De Grandpré, L. (2005). Structural development following fire in black spruce boreal forest. *Forest Ecology and Management*, *206*, 293–306.

Heinselman, M. L. (1981). Fire and succession in the conifer forests of northern North America. In D. C. West, H. H. Shugart, & D. B. Botkin (Eds.), *Forest Succession: Concepts and Application*. (pp. 374–405)Berlin: Springer-Verlag.

Hermosilla, T., Wulder, M. A., White, J. C., Coops, N. C., & Hobart, G. W. (2015). An integrated Landsat time series protocol for change detection and generation of annual gap-free surface reflectance composites. *Remote Sensing of Environment*, *158*, 220–234.

Hopkinson, C., Wulder, M.A., Coops, N.C., Milne, T., Fox, A., & Bater, C.W. (2011). Airborne lidar sampling of the Canadian boreal forest: Planning, execution, and initial processing. *Proceedings of the SilviLaser 2011 conference*.

Huang, C., Goward, S.N., Masek, J.G., Thomas, N., Zhu, Z., & Vogelmann, J.E. (2010). An automated approach for reconstructing recent forest disturbance history using dense Landsat time series stacks. *Remote Sensing of Environment*, *114*, 183–198.

Jennings, S.B., Brown, N.D., & Sheil, D. (1999). Assessing forest canopies and understorey illumination: Canopy closure, canopy cover and other measures. *Forestry*, *72*, 59–73.

Johnstone, J.F., & Chapin, F.S. (2006). Fire interval effects on successional trajectory in boreal forests of northwest Canada. *Ecosystems*, *9*, 268–277.

Johnstone, J.F., Chapin, F.S., III, Foote, J., Kemmett, S., Price, K., & Viereck, L. (2004). Decadal observations of tree regeneration following fire in boreal forests. *Canadian Journal of Forest Research*, *34*, 267–273.

Johnstone, J.F., Hollingsworth, T.N., Chapin, F.S., III, & Mack, M.C. (2010). Changes in fire regime break the legacy lock on successional trajectories in Alaskan boreal forest. *Global Change Biology*, *16*, 1281–1295.

Kane, V.R., Bakker, J.D., McGaughey, R.J., Lutz, J.A., Gersonde, R.F., & Franklin, J.F. (2010). Examining conifer canopy structural complexity across forest ages and elevations with LiDAR data. *Canadian Journal of Forest Research*, *40*, 774–787.

Kane, V.R., Gersonde, R.F., Lutz, J.A., McGaughey, R.J., Bakker, J.D., & Franklin, J.F. (2011). Patch dynamics and the development of structural and spatial heterogeneity in Pacific Northwest forests. *Canadian Journal of Forest Research*, *41*, 2276–2291.

Kane, V.R., Lutz, J.A., Roberts, S.L., Smith, D.F., McGaughey, R.J., Povak, N.A., et al. (2013). Landscape-scale effects of fire severity on mixed-conifer and red fir forest structure in Yosemite National Park. *Forest Ecology and Management*, *287*, 17–31.

Kane, V.R., McGaughey, R.J., Bakker, J.D., Gersonde, R.F., Lutz, J.A., & Franklin, J.F. (2010). Comparisons between field- and LiDAR-based measures of stand structural complexity. *Canadian Journal of Forest Research*, *40*, 761–773.

Kane, V.R., North, M.P., Lutz, J.A., Churchill, D.J., Roberts, S.L., Smith, D.F., et al. (2014). Assessing fire effects on forest spatial structure using a fusion of Landsat and airborne LiDAR data in Yosemite National Park. *Remote Sensing of Environment*, *151*, 89–101.

Kennedy, R.E., Yang, Z., & Cohen, W.B. (2010). Detecting trends in forest disturbance and recovery using yearly Landsat time series: 1. LandTrendr — Temporal segmentation algorithms. *Remote Sensing of Environment*, *114*, 2897–2910.

Lefsky, M.A., Hudak, A.T., Cohen, W.B., & Acker, S.A. (2005). Patterns of covariance between forest stand and canopy structure in the Pacific Northwest. *Remote Sensing of Environment*, *95*, 517–531.

Lefsky, M.A., Turner, D.P., Guzy, M., & Cohen, W.B. (2005). Combining lidar estimates of aboveground biomass and Landsat estimates of stand age for spatially extensive validation of modeled forest productivity. *Remote Sensing of Environment*, *95*, 549–558.

Lentile, L.B., Holden, Z.A., Smith, A.M.S., Falkowski, M.J., Hudak, A.T., Morgan, P., et al. (2006). Remote sensing techniques to assess active fire characteristics and post-fire effects. *International Journal of Wildland Fire*, *15*, 319–345.

Lieffers, V.J., Messier, C., Burton, P.J., Ruel, J. -C., & Grover, B.E. (2003). Nature-based silviculture of sustaining a variety of boreal forest values. In P.J. Burton, C. Messier, D.W. Smith, & W.L. Adamowicz (Eds.), *Towards sustainable management of the boreal forest* (pp. 481–550). Ottawa, Canada: N.R.C. Press.

López García, M.J., & Caselles, V. (1991). Mapping burns and natural reforestation using Thematic Mapper data. *Geocarto International*, *6*, 31–37.

Magnussen, S., & Wulder, M.A. (2012). Post-fire canopy height recovery in Canada's boreal forests using Airborne Laser Scanner (ALS). *Remote Sensing*, *4*, 1600–1616.

Masek, J.G., Vermote, E.F., Saleous, N.E., Wolfe, R., Hall, F.G., Huemmrich, K.F., et al. (2006). A Landsat surface reflectance dataset for North America, 1990–2000. *IEEE Geoscience and Remote Sensing Letters*, *3*, 68–72.

Meigs, G.W., Kennedy, R.E., & Cohen, W.B. (2011). A Landsat time series approach to characterize bark beetle and defoliator impacts on tree mortality and surface fuels in conifer forests. *Remote Sensing of Environment*, *115*, 3707–3718.

Næsset, E. (2004). Practical large-scale forest stand inventory using a small-footprint airborne scanning laser. *Scandinavian Journal of Forest Research*, *19*, 164–179.

Oliver, C. D., & Larson, B. C. (1996). Forest Stand Dynamics. *Update edition*. (pp. 520)New York: Wiley.

Pflugmacher, D., Cohen, W.B., Kennedy, R.E., & Yang, Z. (2014). Using Landsat-derived disturbance and recovery history and lidar to map forest biomass dynamics. *Remote Sensing of Environment*, *151*, 124–137.

Schroeder, T.A., Wulder, M.A., Healey, S.P., & Moisen, G.G. (2011). Mapping wildfire and clearcut harvest disturbances in boreal forests with Landsat time series data. *Remote Sensing of Environment*, *115*, 1421–1433.

Sirois, L., & Payette, S. (1989). Postfire black spruce establishment in subarctic and boreal Quebec. *Canadian Journal of Forest Research*, *19*, 1571–1580.

Song, C., & Woodcock, C.E. (2003). Monitoring forest succession with multitemporal Landsat images: Factors of uncertainty. *IEEE Transactions on Geoscience and Remote Sensing*, *41*, 2557–2567.

Soverel, N.O., Perrakis, D.D.B., & Coops, N.C. (2010). Estimating burn severity from Landsat dNBR and RdNBR indices across western Canada. *Remote Sensing of Environment*, *114*, 1896–1909.

Statistics-Canada (2010). *Road network file*. Ottawa, Canada: Reference Guide.

Stinson, G., Kurz, W.A., Smyth, C.E., Neilson, E.T., Dymond, C.C., Metsaranta, J.M., et al. (2011). An inventory-based analysis of Canada's managed forest carbon dynamics, 1990 to 2008. *Global Change Biology*, *17*, 2227–2244.

Stocks, B.J., Mason, J.A., Todd, J.B., Bosch, E.M., Wotton, B.M., Amiro, B.D., et al. (2002). Large forest fires in Canada, 1959–1997. *Journal of Geophysical Research*, *107*. http://dx.doi.org/10.1029/2001JD000484.

Tucker, C.J. (1979). Red and photographic infrared linear combinations for monitoring vegetation. *Remote Sensing of Environment*, *8*, 127–150.

USDA Forest Service (2003). *Field procedures for the Coastal Alaska Inventory*.

Van Ewijk, K.Y., Treitz, P.M., & Scott, N.A. (2011). *Characterizing forest succession in central Ontario using lidar-derived indices*, *77*. (pp. 261–269), 261–269.

Viereck, L. A. (1983). The effects of fire in black spruce ecosystems of Alaska and Northern Canada. In R. W. Wein, & D. A. MacLean (Eds.), *The role of fire in northern circumpolar ecosystems*. (pp. 201–220)New York, New York, USA: John Wiley and Sons.

Vogelmann, J.E., & Rock, B.N. (1988). Assessing forest damage in high-elevation coniferous forests in Vermont and New Hampshire using Thematic Mapper data. *Remote Sensing of Environment*, *24*, 227–246.

White, J.C., Wulder, M.A., Hobart, G.W., Luther, J.E., Hermosilla, T., Griffiths, P., et al. (2014). Pixel-based image compositing for large-area dense time series applications and science. *Canadian Journal of Remote Sensing*, *40*, 192–212.

Wilson, E.H., & Sader, S.A. (2002). Detection of forest harvest type using multiple dates of Landsat TM imagery. *Remote Sensing of Environment*, *80*, 385–396.

Wooster, M.J. (2004). Boreal forest fires burn less intensely in Russia than in North America. *Geophysical Research Letters*, *31* (L20505).

Wulder, M.A., Masek, J.G., Cohen, W.B., Loveland, T.R., & Woodcock, C.E. (2012). Opening the archive: How free data has enabled the science and monitoring promise of Landsat. *Remote Sensing of Environment*, *122*, 2–10.

Wulder, M.A., White, J.C., Alvarez, F., Han, T., Rogan, J., & Hawkes, B. (2009). Characterizing boreal forest wildfire with multi-temporal Landsat and LIDAR data. *Remote Sensing of Environment*, *113*, 1540–1555.

Wulder, M.A., White, J.C., Bater, C.W., Coops, N.C., Hopkinson, C., & Chen, G. (2012). Lidar plots — A new large-area data collection option: Context, concepts, and case study. *Canadian Journal of Remote Sensing*, *38*, 600–618.

Wulder, M.A., White, J.C., Cranny, M., Hall, R.J., Luther, J.E., Beaudoin, A., et al. (2008). Monitoring Canada's forests. Part 1: Completion of the EOSD land cover project. *Canadian Journal of Remote Sensing*, *34*, 549–562.

Zhu, Z., & Woodcock, C.E. (2012). Object-based cloud and cloud shadow detection in Landsat imagery. *Remote Sensing of Environment*, *118*, 83–94.

Zhu, Z., Woodcock, C.E., & Olofsson, P. (2012). Continuous monitoring of forest disturbance using all available Landsat imagery. *Remote Sensing of Environment*, *122*, 75–91.

Zimble, D.A., Evans, D.L., Carlson, G.C., Parker, R.C., Grado, S.C., & Gerard, P.D. (2003). Characterizing vertical forest structure using small-footprint airborne lidar. *Remote Sensing of Environment*, *87*, 171–182.

Please cite this article as: Bolton, D.K., et al., Characterizing residual structure and forest recovery following high-severity fire in the western boreal of Canada using Landsat t..., *Remote Sensing of Environment* (2015), http://dx.doi.org/10.1016/j.rse.2015.03.004